frontiers in Marine Science

ORIGINAL RESEARCH
published: 21 December 2021
doi: 10.3389/fmars.2021.760909

The Importance of Ecological Accommodation Space and Sediment Supply for Cold-Water Coral Mound Formation, a Case Study From the Western Mediterranean Sea

Haozhuang Wang[1]†, Jürgen Titschack[1,2], Claudia Wienberg[1], Chelsea Korpanty[1] and Dierk Hebbeln[1]*

[1] MARUM – Center for Marine Environmental Sciences, University of Bremen, Bremen, Germany, [2] Senckenberg am Meer, Marine Research Department, Wilhelmshaven, Germany

OPEN ACCESS

Edited by:
Lorenzo Angeletti,
Institute of Marine Science, National Research Council (CNR), Italy

Reviewed by:
Ann I. Larsson,
University of Gothenburg, Sweden
Laurence Helene De Clippele,
University of Edinburgh, United Kingdom

***Correspondence:**
Haozhuang Wang
hwang147@tongji.edu.cn

†Present address:
Haozhuang Wang,
State Key Laboratory of Marine Geology, Tongji University, Shanghai, China

Specialty section:
This article was submitted to Deep-Sea Environments and Ecology, a section of the journal Frontiers in Marine Science

Received: 19 August 2021
Accepted: 01 December 2021
Published: 21 December 2021

Citation:
Wang H, Titschack J, Wienberg C, Korpanty C and Hebbeln D (2021) The Importance of Ecological Accommodation Space and Sediment Supply for Cold-Water Coral Mound Formation, a Case Study From the Western Mediterranean Sea. Front. Mar. Sci. 8:760909. doi: 10.3389/fmars.2021.760909

The formation of cold-water coral (CWC) mounds is commonly seen as being the result of the sustained growth of framework-forming CWCs and the concurrent supply and deposition of terrigenous sediments under energetic hydrodynamic conditions. Yet only a limited number of studies investigated the complex interplay of the various hydrodynamic, sedimentological and biological processes involved in mound formation, which, however, focused on the environmental conditions promoting coral growth. Therefore, we are still lacking an in-depth understanding of the processes allowing the on-mound deposition of hemipelagic sediments, which contribute to two thirds of coral mound deposits. To investigate these processes over geological time and to evaluate their contribution to coral mound formation, we reconstructed changes in sediment transport and deposition by comparing sedimentological parameters (grain-size distribution, sediment composition, accumulation rates) of two sediment cores collected from a Mediterranean coral mound and the adjacent seafloor (off-mound). Our results showed that under a turbulent hydrodynamic regime promoting coral growth during the Early Holocene, the deposition of fine siliciclastic sediments shifted from the open seafloor to the coral mounds. This led to a high average mound aggradation rate of >130 cm kyr^{-1}, while sedimentation rates in the adjacent off-mound area at the same time did not exceed 10 cm kyr^{-1}. Thereby, the baffling of suspended sediments by the coral framework and their deposition within the ecological accommodation space provided by the corals seem to be key processes for mound formation. Although, it is commonly accepted that these processes play important roles in various sedimentary environments, our study provided for the first time, core-based empirical data proving the efficiency of these processes in coral mound environment. In addition, our approach to compare the grain-size distribution of the siliciclastic sediments deposited concurrently on a coral mound and on the adjacent seafloor

allowed us to investigate the integrated influence of coral mound morphology and coral framework on the mound formation process. Based on these results, this study provides the first conceptual model for coral mound formation by applying sequence stratigraphic concepts, which highlights the interplay of the coral-framework baffling capacity, coral-derived ecological accommodation space and sediment supply.

Keywords: cold-water coral mound formation, sediment deposition, baffling capacity, ecological accommodation space, lateral sediment supply

INTRODUCTION

Cold-water coral (CWC) mounds are common and prominent sedimentary features along the upper and mid continental slopes (200–1,000 m water depths) in the Atlantic Ocean and the adjacent marginal seas (e.g., Roberts et al., 2006; Wheeler et al., 2007; Hebbeln and Samankassou, 2015; Wienberg and Titschack, 2017; Lo Iacono et al., 2018). They rise up to several tens and even hundreds of meters above the seafloor (e.g., Mienis et al., 2006) and cluster in provinces often comprising hundreds of individual mounds (e.g., Colman et al., 2005; Wheeler et al., 2007; Glogowski et al., 2015; Hebbeln, 2019; Tamborrino et al., 2019; Steinmann et al., 2020). Coral mound formation results from the complex interplay between sustained growth of framework-forming CWCs and the concurrent supply and deposition of sediments under energetic hydrodynamic conditions (Roberts et al., 2006, 2009). Previous studies on coral mound formation mainly concentrated on the CWCs and the environmental factors supporting their proliferation, such as distinct physical and chemical properties of the ambient water masses (e.g., temperature, dissolved oxygen concentrations, pH, and water density; e.g., Freiwald, 2002; Davies et al., 2008; Davies and Guinotte, 2011; Flögel et al., 2014) and the supply of food by vertical fluxes triggered by surface ocean productivity and horizontal fluxes triggered by strong bottom-water hydrodynamics (e.g., Thiem et al., 2006; Mienis et al., 2007, 2012; Davies et al., 2009; Hebbeln et al., 2016; De Clippele et al., 2018). However, with this strong focus on the CWCs, only one prerequisite for mound formation was considered. The importance of the sediments deposited between the coral framework is often neglected, even though they usually contribute two thirds or more to coral mound deposits (e.g., Dorschel et al., 2007a; van der Land et al., 2014; Titschack et al., 2015). Besides the supply of sufficient sediments, the local deposition of sediments on top of a coral mound, where commonly an energetic hydrodynamic regime prevails (Frederiksen et al., 1992; Dorschel et al., 2007b; Mohn et al., 2014; Juva et al., 2020), depends primarily on the CWC frameworks that reduce the velocity of near-bottom currents and allow bypassing suspended sediments to settle between their branches, a process also known as baffling (e.g., Dorschel et al., 2007b; Guihen et al., 2013). Baffling by coral frameworks is well known and described from tropical shallow-water reefs (e.g., Hallock, 1997), and is also suspected to play an important role for coral mound formation in the deep sea (e.g., Mullins et al., 1981; Foubert et al., 2008; Huvenne et al., 2009; Mienis et al., 2009a; Victorero et al., 2016). For instance, comparing surface sediments from coral mounds and near-by seafloor settings already revealed a relative enrichment of fine material on the mounds that was assumed to reflect (a) the winnowing of fine sediments from the seafloor next to the mounds and (b) their subsequent deposition on the mounds forced by coral baffling (Mullins et al., 1981; Paull et al., 2000; Wheeler et al., 2011). In addition, experimental and modeling studies have impressively shown how current velocities are reduced within CWC frameworks favoring the settlement of suspended sediments (e.g., Chang et al., 2009; Mienis et al., 2019; Bartzke et al., 2021; Hennige et al., 2021). However, detailed studies on the processes controlling sediment delivery and deposition on coral mounds and their impact on coral mound formation, notably over longer timescales, are still largely lacking.

In this study, we investigated the importance of coral baffling and sediment supply for coral mound formation on geological timescales. Therefore, we assessed differences in grain-size distribution, composition and accumulation rates of siliciclastic sediments deposited contemporaneously in two well-dated sediment cores, one obtained from a coral mound in the western Mediterranean (Alborán Sea, East Melilla coral mound province) recording a pronounced Early Holocene mound formation period, and one from the adjacent seafloor displaying slope sedimentation before, during and after this episode in mound formation. In concert with coral preservation patterns within the coral mound core, these data were used to decipher the hydrodynamic and sedimentary processes that prevailed in the respective settings (a) to prove the importance of the coral baffling capacity for mound formation, and (b) to apply, for the first time, sequence stratigraphic concepts to conceptually describe coral mound formation as an interplay between sediment supply and ecological accommodation space (sensu Pomar, 2001; Pomar and Haq, 2016). In this sense, the baffling capacity is defined as the capacity of a coral framework to create a local low energy environment, which allows current-transported sediments to settle even under generally turbulent background conditions (e.g., Ginsburg and Lowenstam, 1958; Flügel, 2004; Titschack et al., 2009), whereas the ecological accommodation space describes the space generated by the coral frameworks that is available for sediment deposition.

MATERIALS AND METHODS

Two gravity cores were investigated within this study, which were retrieved from the East Melilla coral mound province in the southern Alborán Sea (western Mediterranean) during RV

Poseidon cruise POS 385 (Hebbeln et al., 2009). The on-mound core GeoB13729-1 was collected at ∼440 m water depth (**Table 1**) from the western flank of an elongated ridge-like coral mound (named Brittlestar Ridge I; **Figure 1**). This large coral ridge has a maximum elevation of 150 m above the seafloor (for further details see Hebbeln, 2019), and is currently bathed by the Levantine Intermediate Water flowing with velocities of up to 14 cm s^{-1} from east to west at water depths of 200–600 m (Millot and Taupier-Letag, 2005). The on-mound core has a recovery of 447 cm and contains coral fragments of various preservation states throughout the core (see Titschack et al., 2016). Previously published coral ages obtained from this core determined by accelerator mass spectrometry (AMS) radiocarbon (^{14}C) dating revealed a pronounced mound formation phase during the Early Holocene (11.2–9.8 kyr BP; Fink et al., 2013). The off-mound core GeoB13731-1 is 431-cm-long and was collected at 360 m water depth about 4 km southeast of the coral ridge I from the southward shallowing continental slope (**Figure 1** and **Table 1**). A previously established age model (based on seven AMS^{14}C dates of mixed planktonic foraminifera) suggests that the core sediments were deposited during the last ∼23 kyr (for details see Fink et al., 2013).

AMS^{14}C Age Calibration, U/Th Dating on Coral Fragments and Calculation of Sedimentation and Mound Aggradation Rates

For this study, all previously published conventional AMS^{14}C ages obtained for the on- and off-mound cores (see Fink et al., 2013) were re-calibrated using the software CALIB8.2 (Stuiver et al., 2021[1]; **Table 2A**). For the re-calibration, we have applied the MARINE20 calibration curve (Heaton et al., 2021) with a local reservoir age correction of $\Delta R = -90 \pm 80$ years accounting for a deglacial to Holocene marine reservoir age of $R = 370 \pm 40$ years (according to Siani et al., 2000; Reimer and McCormac, 2002; Siani et al., 2011).

For the on-mound core, ten additional coral fragments were sampled from various core depths for Uranium-Thorium (U/Th) dating to improve the existing age model of this core. The coral fragments were mechanically and chemically cleaned according to the procedure described by Frank et al. (2004), and measurements were performed according to the procedures described in detail by Wefing et al. (2017). Sample preparation, chemical purification of the Th and U fractions, and mass spectrometric analyses were carried out at the Institute for Environmental Physics (IUP, University of Heidelberg, Germany) using a multi-collector inductivity coupled plasma mass spectrometer (Thermo Fisher Neptune plus). Absolute U/Th dates are reported as kyr BP (**Table 2B**) in order to compare them with the AMS^{14}C coral ages.

Sedimentation rates (SRs) for the off-mound core were (re-)calculated based on a linear interpolation between the ages (**Table 3**). Also, for the calculation of the mound aggradation rates (ARs) for the on-mound core, an age-to-age calculation was applied, whenever coral ages revealed a strict chronological order. SRs and ARs are given in centimeters per kiloyear (cm kyr^{-1}; **Table 3**).

[1]http://calib.org/calib/calib.html

Grain-Size Analyses

For the off-mound core GeoB13731-1, grain-size distribution data of the siliciclastic sediment fraction were already published by Fink et al. (2013). The sampling resolution was 10 cm and analyses were performed with a Beckman Coulter LS200 (for further details see Fink et al., 2013). For this study, additional samples (per sample ∼1–2 g of bulk sediment) were collected from the off-mound core from the core depth interval of 318–338 cm in 2-cm-resolution, which, according to the existing age model, temporally corresponds to the Early Holocene mound formation period that is represented by the on-mound core GeoB13729-1 (Fink et al., 2013). Further samples for grain-size analyses were collected from the matrix sediments (per sample ∼1–2 g of sediment without coral fragments) of the on-mound core in 10-cm-resolution throughout the core. For all sediment samples (off- and on-mound cores), the biogenic components (organic carbon, carbonate, and biogenic opal) were removed prior to the grain-size analyses following the protocol of Fink et al. (2013). During the entire preparation, deionized, degassed and filtered water (mesh size of 0.2 μm) was used to reduce the potential influence of air bubbles or particles in the water. The new set of sediment samples was measured in the Particle-Size laboratory at MARUM (University of Bremen, Germany) using a Beckman Coulter LS13320. To be consistent with the data of Fink et al. (2013), only the size range between 0.4 and 2,000 μm, divided into the same 92 size classes, was used. Results are provided in volume percentages (vol.%) of the specific size classes.

Dry Bulk Density Measurements

Sediment dry bulk density measurements were conducted on the sediments of the off-mound core GeoB13731-1 and on the matrix sediments of the on-mound core GeoB13729-1 in 10-cm-resolution. Approximately 8 cm^3 of material were wet weighed and subsequently dried for 24 h within a convection oven at temperatures of 100–110°C. After cooling to room temperature in a desiccator, sediment volumes were measured with a PentaPyc 5200e gas pycnometer (Quantachrome instruments) in the Geotechnical Laboratory at MARUM, University or Bremen, Germany. The dry bulk density was determined by following the ODP methodology of Blum (1997).

Total Carbon, Total Organic Carbon, and $CaCO_3$ Determinations

Total carbon (TC) and total organic carbon (TOC) contents (in wt.%) of the sediments of off-mound core GeoB13731-1 and the matrix sediments of on-mound core GeoB13729-1 were analyzed in 10- and 5-cm-resolution, respectively. Prior to the analyses, the freeze-dried (matrix) sediments were first ground, and then divided into two subsamples of approximately 50 mg each to determine TC and TOC. For the TOC measurements, the total inorganic carbon was removed with 12.5% HCl prior to the

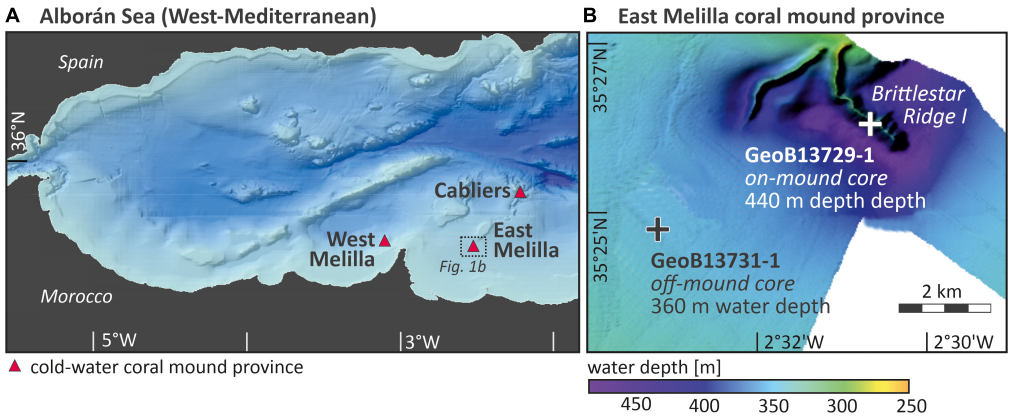

FIGURE 1 | (A) Overview map showing the Alborán Sea in the western Mediterranean. Coral mound provinces are indicated by a red triangle. **(B)** Bathymetry map of the northern East Melilla cold-water coral mound province in the southern Alborán Sea showing the locations of the sediment cores used for this study (off-mound: GeoB13731-1, on-mound: GeoB13729-1). Map modified from Hebbeln (2019).

TABLE 1 | Metadata of gravity cores collected from the East Melilla coral mound province (southern Alborán Sea) during the cruise POS 385 with the German RV Poseidon in 2009 (Hebbeln et al., 2009). Indicated are also analyses which were applied to the core sediments. Some data of these analyses were previously published in Fink et al. (2013) and Titschack et al. (2016), while others were newly obtained for this study. REC: core recovery, CT: computer tomography, TC: total carbon, TOC: total organic carbon, $CaCO_3$: carbonate.

Core metadata					Core analyses					
Core-ID (GeoB)	**Latitude (N)**	**Longitude (S)**	**Depth (m)**	**REC (cm)**	**AMS^{14}C Dating**	**Th/U Dating**	**CT Scans**	**Grain Size**	**Dry bulk Density**	**TC, TOC $CaCO_3$**
13731-1 *off-mound*	35°24.80′	2°33.22′	362	431	7x [1]	/	/	X [1,3]	X [3]	X [3]
13729-1 *on-mound*	35°26.07′	2°30.83′	442	447	5x [1]	10x [3]	X [2]	X [3]	X [3]	X [3]

Source of original data: [1] Fink et al. (2013); [2] Titschack et al. (2016); [3] this study.

analysis. Both subsamples (for TC and TOC) were measured with a Leco CS 200 at the Department of Geosciences, University of Bremen, Germany. Later on, the $CaCO_3$ content was calculated following the standard equation:

$$CaCO_3[\text{wt.\%}] = (TC - TOC)[\text{wt.\%}] \times 8.333$$

with the factor 8.333 representing the molecular weight ratio of $CaCO_3$ and carbon (e.g., Faust et al., 2020; Tapia et al., 2021).

Calculation of Sediment Composition and Associated Accumulation Rates

For the off-mound core, the sediment composition was assessed on the basis that it consists of three main components: siliciclastic material, carbonate, and organic carbon. Consequently, the relative contribution of siliciclastic material (Silic) was calculated as

$$Silic_{off}[\text{wt.\%}] = 100[\text{wt.\%}] - CaCO_{3\,off}[\text{wt.\%}] - TOC_{off}[\text{wt.\%}]$$

The main difference in sediment composition between the on- and the off-mound cores are the corals within the on-mound core. The coral content per volume ($C_{Coral-V}$ [vol.%]) for the on-mound core is provided by Titschack et al. (2016) based on computer tomography (CT). For analyzing the composition of the matrix sediments of the on-mound core, the same approach as for the off-mound core was applied. However, for the assessment of the overall sediment composition, these had to be combined with the coral content to calculate the individual contributions as exemplified here for the siliciclastic material

$$Silic_{on}[\text{wt.\%}] = \frac{(100\,[\text{vol.\%}] - C_{Coral-v}) \times \rho_{matrix} \times \text{matrix } Silic_{on}[\text{wt.\%}]}{(100\,[\text{vol.\%}] - C_{Coral-v}) \times \rho_{matrix} + C_{Coral-v} \times \rho_{coral}}$$

with ρ_{matrix} corresponding to the measured dry bulk density of the matrix sediments and ρ_{coral} (2.66 g cm^{-3}) to the density of coral skeletons (see Dorschel et al., 2007a). The weight percentage of organic carbon (TOC_{on} [wt.%]) and carbonate ($CaCO_{3on}$ [wt.%]) were calculated by substituting the matrix $Silic_{on}$ [wt.%] by the matrix TOC_{on} [wt.%] and matrix $CaCO_{3on}$ [wt.%] in the above equation.

TABLE 2 | (A) AMS^{14}C dates obtained from mixed planktonic foraminifera (PLF) of the off-mound core GeoB13731-1 and from cold-water coral fragments (*Lophelia pertusa* a.k.a. *Desmophyllum pertusum*) of the on-mound core GeoB13729-1. The AMS^{14}C ages were corrected for ^{13}C and converted into calendar ages using with CALIB 8.20 (Stuiver et al., 2021; http://calib.org/calib/calib.html). For the calibration of the conventional AMS^{14}C, the MARINE 20 calibration curve has been applied (Heaton et al., 2021) with a local reservoir age correction of $\Delta R = -90 \pm 80$ years accounting for a deglacial to Holocene marine reservoir age of $R = 370 \pm 40$ years (according to Siani et al., 2000; Reimer and McCormac, 2002; Siani et al., 2011). SD: sampling depth, MPA: median probability age. **(B)** U/Th dates obtained from cold-water coral fragments (*L. pertusa*) of the on-mound core GeoB13729-1. Provided are 232Th concentrations and decay corrected ^{234}U/^{238}U activity ratios [δ^{234}U(i)] calculated from the given ages and with λ^{234}U: 2.82206 (±0.00302) × 10^{-6}yr^{-1}). The age at 331 cm core depth is marked in italics as it is most likely affected by diagenetic alternation as indicated by the high ^{232}Th concentration.

A

Core ID (GeoB)	SD (cm)	Material	Lab code	Conv. ^{14}C age (kyr)	1σ (kyr)	2σ range cal. age (kyr BP)		MPA (kyr BP)	2σ (kyr BP)
off-mound									
13731-1	8	mixed PLF	UCIAMS-78807	0.550	0.015	0	0.279	0.120	0.120
13731-1	128	mixed PLF	UCIAMS-78808	2.005	0.015	1.292	1.713	1.500	0.210
13731-1	203	mixed PLF	UCIAMS-78809	4.035	0.015	3.723	4.261	4.000	0.270
13731-1	328	mixed PLF	UCIAMS-78810	9.480	0.020	10.031	10.554	10.280	0.250
13731-1	353	mixed PLF	UCIAMS-78811	11.630	0.025	12.809	13.253	13.040	0.230
13731-1	368	mixed PLF	UCIAMS-78812	14.775	0.035	16.868	17.464	17.160	0.300
13731-1	423	mixed PLF	UCIAMS-78807	19.345	0.050	22.259	22.843	22.530	0.270
on-mound									
13729-1	2.5	*L. pertusa*	UCIAMS-73570	9.085	0.030	9.486	10.048	9.740	0.250
13729-1	49	*L. pertusa*	UCIAMS-73571	9.330	0.025	9.768	10.336	10.070	0.310
13729-1	140	*L. pertusa*	UCIAMS-73572	9.705	0.025	10.249	10.880	10.580	0.330
13729-1	315	*L. pertusa*	UCIAMS-73573	9.935	0.030	10.632	11.180	10.910	0.280
13729-1	375	*L. pertusa*	UCIAMS-73574	10.225	0.030	11.064	11.628	11.310	0.240

B

Core ID (GeoB)	SD (cm)	Material	Lab code	^{232}Th (ng/g)	± (abs.)	δ^{234}U(i) (‰)	± (abs.)	Age (kyr BP)	± (kyr BP)
on-mound									
13729-1	21	*L. pertusa*	IUP-10867	0.3541	0.0006	148.9	0.9	8.959	0.024
13729-1	74	*L. pertusa*	IUP-10868	1.4134	0.0021	147.0	0.5	10.422	0.063
13729-1	91	*L. pertusa*	IUP-10869	0.3246	0.0006	147.2	1.1	10.460	0.035
13729-1	159	*L. pertusa*	IUP-10870	0.2809	0.0005	148.7	0.7	10.779	0.031
13729-1	231	*L. pertusa*	IUP-10871	0.2478	0.0004	149.3	0.8	10.930	0.029
13729-1	269	*L. pertusa*	IUP-10872	0.2933	0.0005	149.0	0.5	10.872	0.031
13729-1	331	*L. pertusa*	IUP-10873	*5.1269*	*0.0084*	*147.9*	*0.5*	*10.546*	*0.200*
13729-1	395	*L. pertusa*	IUP-10874	0.3053	0.0007	149.4	0.6	11.437	0.041
13729-1	413	*L. pertusa*	IUP-10875	0.3942	0.0009	150.5	0.6	12.130	0.038
13729-1	426	*L. pertusa*	IUP-10876	0.2344	0.0005	148.9	0.6	12.126	0.038

Subsequently, for the on-mound core, the coral content per weight ($C_{Coral-w}$ [wt.%]) was obtained following the equation:

$$C_{Coral-w}[wt.\%] = 100[wt.\%] - Silic_{on}[wt.\%] - TOC_{on}[wt.\%] - CaCO_{3on}[wt.\%]$$

To assess the accumulation rates of the siliciclastic sediments being in the focus here, especially for the on-mound core, the significant contribution of coral carbonate to the overall accumulation must be considered. In a first step, the total sediment density (ρ_{total}) was obtained by summing up the densities of corals and matrix sediments with respect to their contributions as

$$\rho_{total} = C_{Coral-V} \times \rho_{coral} + (100[vol.\%] - C_{Coral-V}) \times \rho_{matrix}$$

In the second step, the weight contribution of siliciclastic sediments per volume of total sediment (W_{Silic}, g cm^{-3}) was obtained by the equation:

$$W_{Silic} = \rho_{total} \times Silic_{on}[wt.\%]$$

The same approach has been used for the off-mound core.

Finally, accumulation rates of the siliciclastic sediment (Acc_{Silic}) were calculated by multiplying the contribution of siliciclastic sediments per volume of total sediments with the respective SR (for the off-mound core) or AR (for the on-mound core):

$$Acc_{Silic} = W_{Silic} \times SR \; or \; W_{Silic} \times AR.$$

TABLE 3 | Sedimentation rates (SR) calculated for off-mound core GeoB13731-1 and mound aggradation rate (AR) calculated for on-mound core GeoB13729-1 (U/Th dates are marked by an asterisk; note that one coral age at 331 cm core depth (~10.5 kyr BP; given in italic) was disregarded for AR calculation). SD, sampling depth. For further explanation see text.

off-mound					on-mound				
Core ID (GeoB)	**SD (cm)**	**Age (kyr BP)**	**± (kyr BP)**	**SR (cm kyr^{-1})**	**Core ID (GeoB)**	**SD (cm)**	**Age (kyr BP)**	**± (kyr BP)**	**AR (cm kyr^{-1})**
13731-1	8	0.120	0.120	–	13729-1	3	9.740	0.250	
13731-1	128	1.500	0.210	87	13729-1	21	8.959*	0.024	
13731-1	203	4.000	0.270	30	13729-1	49	10.070	0.310	41
13731-1	328	10.280	0.250	20	13729-1	74	10.422*	0.063	71
13731-1	353	13.040	0.230	9	13729-1	91	10.460*	0.035	447
13731-1	368	17.160	0.300	4	13729-1	140	10.580	0.330	408
13731-1	423	22.530	0.270	10	13729-1	159	10.779*	0.031	95
average SR: ~19 cm kyr^{-1}					13729-1	231	10.930*	0.029	
					13729-1	269	10.872*	0.031	
					13729-1	315	10.910	0.280	1033
					13729-1	*331*	*10.546**	*0.200*	
					13729-1	375	11.310	0.240	158
					13729-1	395	11.437*	0.041	157
					13729-1	413	12.130*	0.038	
					13729-1	426	12.126*	0.038	45
					average AR: ~133 cm kyr^{-1}				

RESULTS

Off-Mound Core GeoB13731-1

Age Model and Sedimentation Rates

The off-mound sediments were deposited during the last ~23 kyr with calculated SRs ranging from 4 to 87 cm kyr^{-1} (average SR: ~19 cm kyr^{-1}). The SRs were rather low with 4 – 10 cm kyr^{-1} before 10.3 kyr BP and remained moderate with values of 20 – 30 cm kyr^{-1} throughout the Holocene. Only since 1.5 kyr BP, the SR reached highest values of 87 cm kyr^{-1} (**Tables 2A**, **3** and **Figure 2**).

Grain-Size Distribution

The grain-size distribution of the siliciclastic sediment fraction showed changing dominant modes throughout the entire core. Before 17.2 kyr BP and since ~9.8 kyr BP, the dominant mode was at ~8 Φ (4 μm) with maximum size fraction contents of 2.3–3.4 vol.% (**Figures 2**, **3**). Between 17.2 and 9.8 kyr BP, the grain-size distribution showed a distinctively different pattern with a dominant mode at ~4 Φ (63 μm) with maximum size fraction contents between 2.2 and 4.9 vol.% (**Figures 2**, **3**).

Sediment Composition

The sediment composition of core GeoB13731-1 was dominated by siliciclastic sediments with contents ranging from 58.2 to 73.0 wt.% (average: 63.9 wt.%; **Figure 2**). Carbonate contributed between 26.2 and 41.2 wt.% (average: 35.3 wt.%), while the organic carbon content was very low (<1.0 wt.%; not displayable in **Figure 2**). Before 9.8 kyr BP, the siliciclastic and carbonate contents showed almost no fluctuations and ranged from 58.2 to 66.0 wt.% and from 33.3 to 41.2 wt.%, respectively (**Figure 2**). Since 9.8 kyr BP, the siliciclastic sediment content slightly increased (59.1 – 68.7 wt.%) and finally reached its highest content (60.3 – 73.0 wt.%) since 1.5 kyr BP (**Figure 2**). On the contrary, the carbonate contents slightly decreased to 30.4 – 40.3 wt.% between 9.8 and 1.5 kyr BP and to 26.2 – 38.8 wt.% since 1.5 kyr BP.

Accumulation Rate of the Siliciclastic Sediment Fraction

The accumulation rate of the siliciclastic sediments (Acc_{Silic}) varied throughout the core between 3 and 59 g cm^{-2} kyr^{-1} (average: 23 g cm^{-2} kyr^{-1}) and showed a trend comparable to the SRs (**Figure 2**). The lowest Acc_{Silic} occurred before 10.3 kyr BP (3 – 7 g cm^{-2} kyr^{-1}; average: 6 g cm^{-2} kyr^{-1}), which tripled between 10.3 and 1.5 kyr BP (12 – 19 g cm^{-2} kyr^{-1}; average: 16 g cm^{-2} kyr^{-1}). Since 1.5 kyr BP, the Acc_{Silic} increased to maximum values of 47 – 59 g cm^{-2} kyr^{-1} (average: 55 g cm^{-2} kyr^{-1}).

On-Mound Core GeoB13729-1

Age Model and Mound Aggradation Rates

The newly obtained U/Th coral ages ranged from 12.1 ± 0.04 to 9 ± 0.02 kyr BP (**Table 2B**), while the re-calibrated AMS^{14}C coral ages ranged from 11.3 ± 0.24 to 9.7 ± 0.25 kyr BP (**Table 2A**). Hence, combining both age data sets revealed that mound formation lasted for ~3 kyr corresponding to the very late Younger Dryas and the Early Holocene. Even though, the U/Th and AMS^{14}C coral ages complement each another, the ages do not always follow a strict chronological order, which had to be considered for the calculation of mound ARs as it partly avoided a strict age-to-age calculation. At core depths of 426–413 cm and 315–231 cm, the coral ages showed a minor dis-chronological order, however, which were within the given age error (**Table 3**).

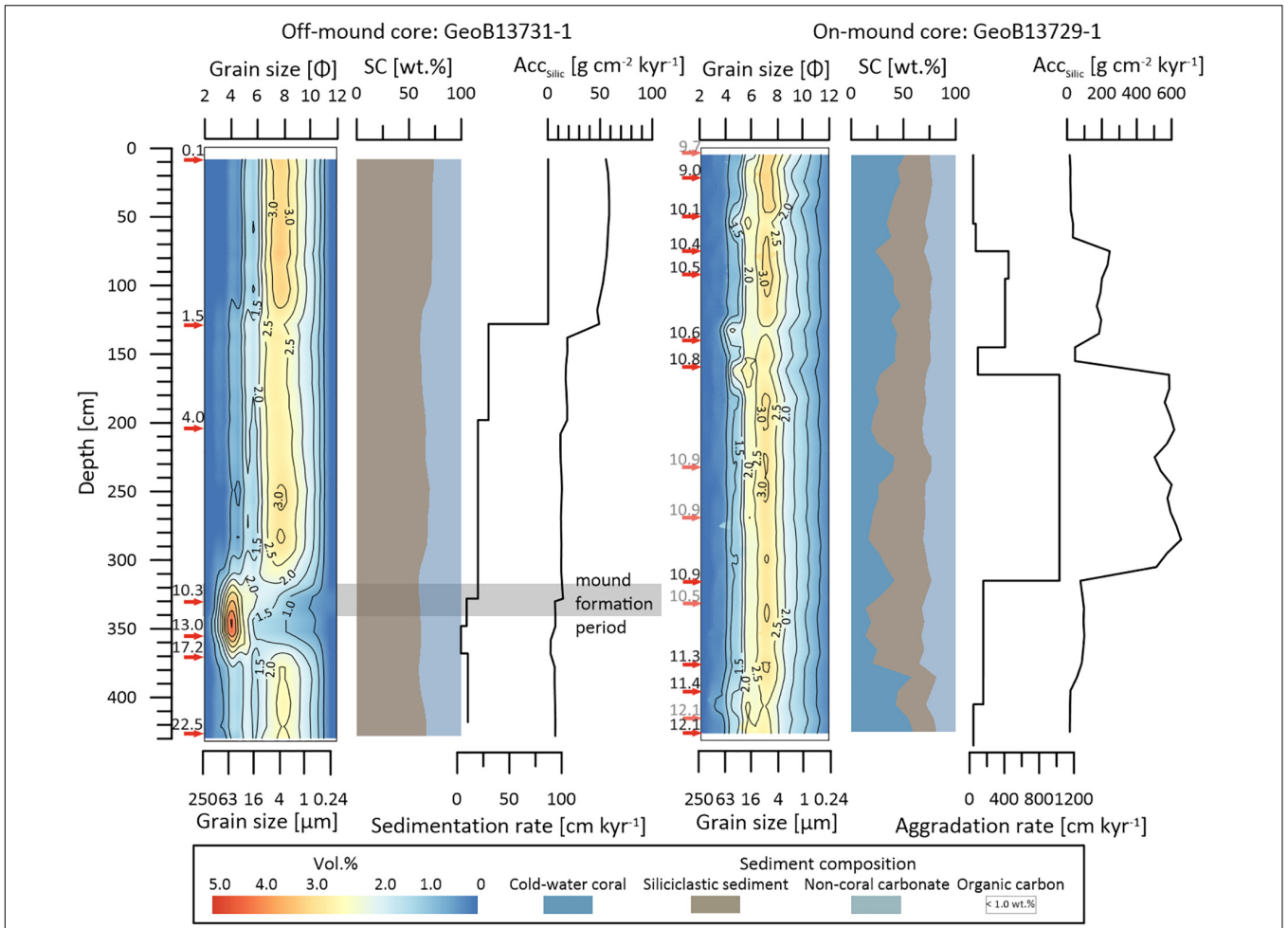

FIGURE 2 | Core logs of the off-mound core GeoB13731-1 and the on-mound core GeoB13729-1. Data obtained from the off-mound core (from left to right): AMS^{14}C dates (indicated by red arrows) obtained from mixed planktonic foraminifera, grain size distribution of siliciclastic sediments, sediment composition (SC), sedimentation rate, and accumulation rate of siliciclastic sediments (Acc$_{Silic}$). The off-mound core interval temporally corresponding to the mound formation period archived in the on-mound core is highlighted by a gray bar (for detailed comparison see also **Figure 3**). Data obtained for the on-mound core (from left to right): AMS^{14}C and U/Th dates (indicated by red arrows) obtained from cold-water coral fragments, grain size distribution of siliciclastic sediments, SC, coral mound aggradation rate, and Acc$_{Silic}$. Coral ages in gray were not used for the calculation of mound aggradation rate. All ^{14}C dates were published by Fink et al. (2013).

Here, we used the oldest and youngest coral ages in relation to the maximum and minimum core depths of the respective core intervals for the AR calculation. The coral age obtained from the core top (9.7 kyr BP) was ∼700 years older than a coral age obtained from a slightly deeper part of the core (21 cm). However, as the upper 10–20 centimeters of a sediment core are commonly disturbed related to the coring procedure and core handling, the younger age likely displays the true age of the core top and was therefore considered for AR calculation. Finally, the U/Th -age of 10.5 kyr BP at 331 cm core depth has been disregarded for AR calculation as it revealed an enhanced ^{232}Th concentration of >5 ng/g (**Table 2B**), which points to diagenetic alteration.

The average AR calculated for the entire ∼3 kyr mound formation period (12.1–9 kyr BP) documented by the on-mound core was ∼133 cm kyr^{-1}, while the ARs varied through time between 40 and 1,040 cm kyr^{-1} (**Table 3**). Highest ARs (100–1,040 cm kyr^{-1}) with an average of 320 cm kyr^{-1} occurred between 11.4 and 10.4 kyr BP, while before and after this period ARs were lower (though still high) with 40–70 cm kyr^{-1} (**Table 3**).

Grain-Size Distribution

The grain-size distribution of the siliciclastic fraction was quite homogenous and no significant variations occurred, not even when the corresponding mound ARs showed distinct variations. Throughout the core, the grain sizes show a dominant mode at ∼7 Φ (8 µm) with maximum size fraction contents of ∼2.2 – 3.3 vol.% (**Figures 2**, **3**).

Sediment Composition

In contrast to the off-mound core, the sediments of the on-mound core not only comprised siliciclastic sediments, carbonate and organic carbon within the matrix sediments, but also coral fragments (**Figure 2**). The carbonate content of the matrix

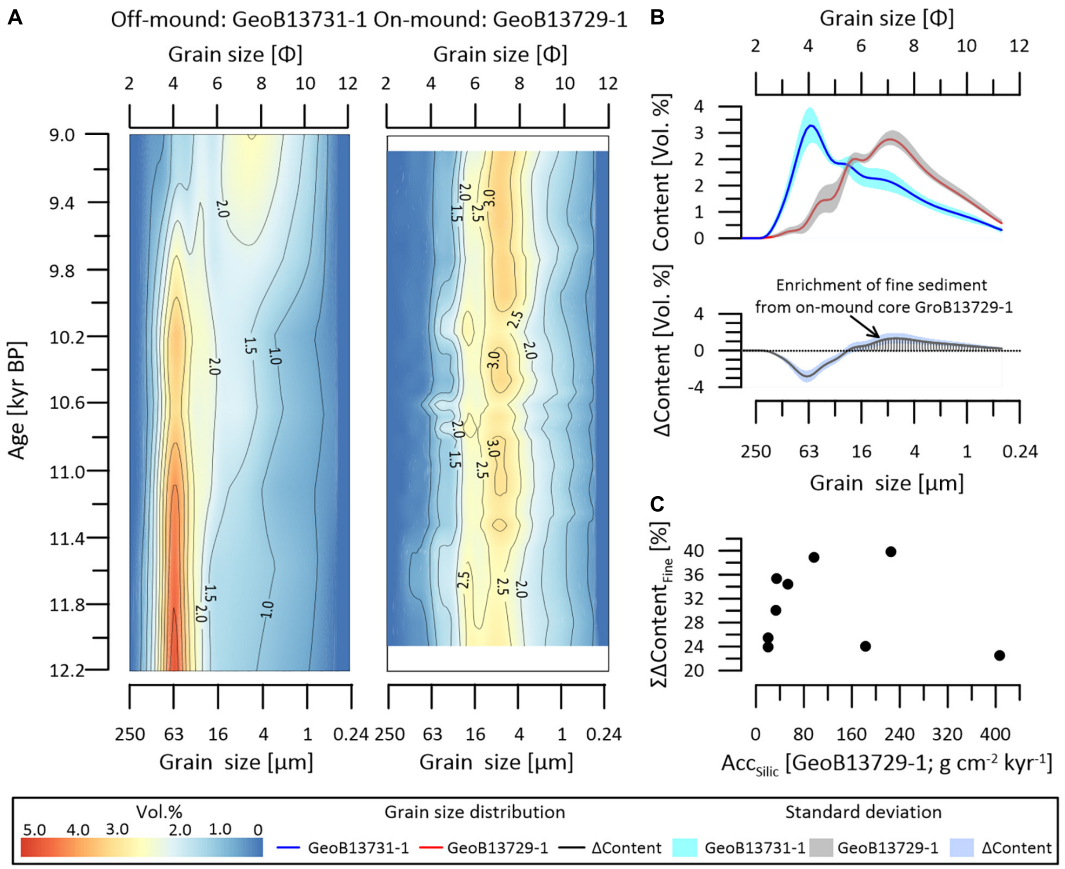

FIGURE 3 | (A) Grain-size distribution of the siliciclastic sediment fraction obtained from the off-mound core GeoB13731-1 and the on-mound core GeoB13729-1 for the mound formation period (~12.1 to 9 kyr BP). **(B)** The averaged grain-size distribution of the two cores. The difference in grain-size distribution between the on- and the off-mound cores (ΔContent) was obtained by subtracting the off-mound core from the on-mound core grain-size distribution. The dashed area represents the averaged total enhancement of the siliciclastic fine fraction ($\Sigma\,\Delta Content_{Fine}$). **(C)** Scatter plot of the $\Sigma\,\Delta Content_{Fine}$ versus accumulation rate of siliciclastic sediments (Acc_{Silic}).

sediments was rather stable, contributing between 19 and 35 wt.% (average: 27 wt.%) to the overall sediment composition. The organic carbon content was very low (<0.7 wt.%; not displayable in **Figure 2**) throughout the entire core. The main variations in sediment composition resulted from changing coral and siliciclastic sediment contents that showed opposing trends through time. Before 11.4 kyr BP, the coral content was high, with values of 42 – 59 wt.% (average: 51 wt.%), whereas the siliciclastic sediment content remained relatively low with values of 22 – 32 wt.% (average: 26 wt.%; **Figure 2**). Between 11.4 and 10.8 kyr BP, the coral content decreased to values in the range of 13 – 41 wt.% (average: 25 wt.%), while the siliciclastic sediment content concurrently increased, contributing between 35 and 53 wt.%. Between~10.8 and ~9.7 kyr BP, the corals and siliciclastic sediments contributed almost equally to the total sediment composition, with values in the range of 22 – 42 wt.% (average: 38 wt.%) and 29 – 47 wt.% (mean: 36 wt.%), respectively. Only at the core top (<9.7 kyr BP), the content of corals (44 – 51 wt. %; average 47 wt.%) dominated again over the siliciclastic sediments (23 – 32 wt.%; average: 28 wt.%; **Figure 2**).

Accumulation Rates of the Siliciclastic Sediment Fraction

The Acc_{Silic} co-varied with the mound AR and ranged in total between 15 and 655 g cm^{-2} kyr^{-1} (average: 260 g cm^{-2} kyr^{-1}). Before 11.4 kyr BP, the Acc_{Silic} was very low, ranging between 16 and 17 g cm^{-2} kyr^{-1}. Between 11.4 and 10.9 kyr BP, the Acc_{Silic} increased to values between 57 and 99 (average: 84 g cm^{-2} kyr^{-1}). The highest values of up to 655 g cm^{-2} kyr^{-1} were obtained between 10.9 and 10.4 kyr BP (average: 425 g cm^{-2} kyr^{-1}) and only dropped once to ~ 45 g cm^{-2} kyr^{-1} at ~10.7 g cm^{-2} kyr^{-1}. Since 10.4 kyr BP, the Acc_{Silic} was again very low, with values in the range of 15 – 34 g cm^{-2} kyr^{-1} (average: 23 g cm^{-2} kyr^{-1}; **Figure 2**).

Difference in Grain-Size Distribution of the Simultaneously Deposited Siliciclastic Sediments in the On- and Off-Mound Cores

Between 17.2 to 9.8 kyr BP, the siliciclastic sediment fraction within the off-mound core exhibited a significant shift of

the major mode to coarser grain sizes (∼4 Φ) compared to the sediments deposited before and after this period (∼8 Φ; **Figure 3B**). In contrast, the on-mound sediments deposited during the mound formation period between 12.1 and 9 kyr BP were constantly dominated by a fine major mode (∼7 Φ; **Figures 2**, **3A**), which is very close to the major mode of the typical off-mound sediments prior to 17.2 kyr BP and after 9.8 kyr BP. Calculating the difference of the average grain-size distributions between the simultaneously deposited siliciclastic sediments (ΔContent) highlights the enrichment of fine sediments (fine silt and clay; $\Delta Content_{Fine}$) in the on-mound core (hatched area in **Figure 3B**). Summing up the enrichments for the relevant size classes reveals an overall enrichment of the siliciclastic fine fraction in the on-mound core ($\Sigma \Delta Content_{Fine}$) in the range of 22 – 40 vol.% (average: 30 vol.%), which shows no clear correlation to the Acc_{Silic} (**Figure 3C**).

DISCUSSION

To elucidate the complex interaction between coral mound morphology, coral framework and sediment supply on the mound formation process, we quantitatively compared the grain-size distribution, sediment composition and accumulation rates of siliciclastic sediments deposited contemporaneously on a coral mound and on the adjacent (off-mound) seafloor. The sedimentological data obtained from the off-mound site (core GeoB13731-1) indicated a pronounced shift to coarse sediments (mode: ∼4 Φ/63 μm) between 17.2 and 9.8 kyr BP, while before and after this time interval fine sediments (mode: ∼8 Φ/4 μm) prevailed (**Figure 2**). This shift to coarser sediments was caused by a significant strengthening of the regional bottom-water hydrodynamics (e.g., geostrophic currents, internal waves). It is supported by the simultaneous deposition of fine sediments on the coral mound, which clearly point to a sediment bypass situation in the area adjacent to the coral mound. A likely related contemporaneously increased supply of sediment (and food) particles was also suggested to be a trigger for the most recent major coral mound formation period documented for various coral mounds in the southern Alborán Sea since the last deglaciation (Fink et al., 2013; Stalder et al., 2015, 2018; Wang et al., 2019; Fentimen et al., 2020; Corbera et al., 2021).

However, in contrast to the off-mound area, the matrix sediments deposited on the coral mound (core GeoB13729-1) investigated in this study showed a homogenous grain-size distribution with a dominant fine mode (∼7 Φ/8 μm) throughout the documented mound formation period between 12.1 and 9 kyr BP, even exhibiting an average ∼30 vol.% - enrichment of the fine fraction in comparison to the concurrently deposited off-mound sediments (**Figure 3**). This points to rather calm hydrodynamic conditions prevailing on top of the coral mound which was capped by dense CWC frameworks that allowed even the fine fraction of the current-transported sediment load to become deposited. At first glance, this conflicts with the reconstructed enhanced hydrodynamics at the near-by seafloor and also contradicts with the common sense that a seafloor obstacle, such as the positive topography of a coral mound, is expected to accelerate bottom-current velocities (e.g., Cyr et al., 2016).

However, flume tank experiments and modeling studies highlighted the remarkable surface roughness of branching corals with large bottom drag coefficients (Monismith, 2007), which significantly slow down bypassing currents, both on colony- and reef-scale (e.g., Chang et al., 2009; Guihen et al., 2013; Johansen, 2014; Lowe and Falter, 2015; Mienis et al., 2019; Bartzke et al., 2021; Hennige et al., 2021). Hence, the baffling capacity of densely distributed coral frameworks on the mound's surface results in a low energy environment allowing fine suspended sediments to settle even under generally turbulent background conditions. With our data, we could confirm that the baffling capacity of a thriving reef represents a very effective sediment trap and is therefore an essential factor for coral mound formation. In combination with very high sediment availability, this led to a remarkably high average on-mound accumulation rate of siliciclastic sediments (Acc_{Silic}: 260 g $cm^{-2}kyr^{-1}$), which was up to ∼25-fold higher compared to the contemporaneous accumulation rate obtained for the adjacent (off-mound) seafloor (Acc_{Silic}: 11 g $cm^{-2}kyr^{-1}$; **Figure 2**).

When comparing the on-mound grain-size distribution data of the siliciclastic sediments with those of the off-mound site obtained before and after the documented mound formation period, the major grain-size modes are very similar (on-mound: at ∼7 Φ/8 μm, off-mound: ∼8 Φ/4 μm; **Figure 2**). This indicates that the sediment transported to our study site in the southern Alborán Sea did not change significantly in its grain-size distribution pattern during the past 23 kyr. Instead, the hydrodynamics, which strengthened during the mound formation period, caused a bypass situation of the fine sediment fraction or even erosion in the off-mound setting, while this could still be baffled by the coral framework and deposited on mound.

Even though our data showed that sediment baffling by coral frameworks represents the prerequisite for any coral mound formation, the rather constant $\Sigma Contenti_{ng}$ ranging between 22 vol.% and 40 vol.% (**Figure 3C**) indicated that the baffling capacity of the coral framework did not vary significantly during the entire mound formation period despite strongly varying (though continuously high) on-mound Acc_{Silic} (**Figure 3C**). This apparent lack in correlation implies that the baffling capacity must have been continuously high but had only a minor influence on the mound AR. Hence, the mound AR was probably rather controlled by changes in sediment supply, which points to another process called sediment focusing, i.e., sediment deposition fed by lateral sediment supply (e.g., Francois et al., 2004), that seems to play a further important role in mound formation. Under a prevailing relatively high-energy environment, most of the delivered sediment was kept in suspension (or even eroded from the seabed). Deposition primarily occurred in the low-energy conditions among the coral branches, resulting in a deposition largely limited to (focused on) the mounds. Thus, sediments, which become deposited in the off-mound area under calm hydrodynamic conditions, were baffled on-mound under more vigorous hydrodynamics. Assuming a rather stable sediment input to the system, as indicated by rather similar grain-size distributions between the on-mound deposits

and the off-mound deposits prior to 17.2 ka BP and after 9.8 ka BP (**Figure 2**), the resulting decrease in accommodation space from the wide off-mound areas to a few coral mounds probably also contributed to the extremely high Acc_{Silic} observed in the on-mound core.

Furthermore, it is important to note that coral mound formation does not solely depend on a high baffling capacity of the coral framework and sediment supply. It depends further on the space generated by the coral frameworks that is available for sediment deposition, defined here as coral-derived ecological accommodation space. Thus, in this sense CWC frameworks on coral mounds act in a similar way as shallow-water carbonate factories (e.g., rhodolith and maerl beds, shallow-water coral reefs; see Riosmena-Rodriguez et al., 2017; Pomar et al., 2017), in which carbonate-producing organisms alter the hydrodynamics by baffling and generate ecological accommodation space for sediment deposition. This ecological accommodation space within the coral frameworks is predominantly controlled by the growth of the corals. Large and densely distributed coral frameworks provide a larger ecological accommodation space compared to small colonies distributed in a rather scattered manner (**Figure 4**). Consequently, changes in mound AR are primarily controlled by the interplay between sediment supply and the coral-derived ecological accommodation space defined by the dimension and density of coral frameworks present on the mound's surface.

For our case study from the Alborán Sea, the contents of corals and siliciclastic sediments displayed in the on-mound core are rather constant through time, although the mound AR and the accumulation rates of both components show major, but parallel changes (**Figure 2**). The mound AR is high (>100 cm kyr^{-1}) for most of the record, which suggests a close-to-optimal interplay of coral growth – providing the ecological accommodation space – and sediment supply. The CT-based coral preservation pattern supports this assumption as coral frameworks that experienced minor breakdown or compaction correlate with ARs of ∼100–300 cm kyr^{-1}, while coral frameworks preserved in life position coincide with ARs of >300 cm kyr^{-1} (see also Titschack et al., 2016). Consequently, minor changes of this close-to-optimal-conditions ratio result in significant changes in mound ARs and sediment accumulation rates. Under these conditions, the hydrodynamic setting might be a key component as stronger currents provide (i) more food for faster growth of a dense coral framework and (ii) deliver more suspended sediments. Both factors increase simultaneously the ecological accommodation space and sediment supply and, thus, are directly reflected in the mound AR.

The important role of the interplay between ecological accommodation space (A) and sediment supply (S) for coral mound formation and coral preservation patterns within mound deposits is revealed, when considering various mound settings described in the literature (see below). This comparison allows the postulation of three major coral mound formation scenarios (**Figure 4**):

Scenario 1: The coral-derived ecological accommodation space considerably exceeds the sediment supply ($A/S >> 1$; **Figure 4A**). The fast and sustained growth of corals forming large, densely distributed frameworks results in a high baffling capacity, provides an increased accommodation space and allows the current-transported sediments to be deposited on the mound. As the sediment supply is low, a large part of the accommodation space remains unfilled and part of (the dead portion of) the coral frameworks is exposed to prolonged bioerosion and fragmentation. This eventually causes the collapse of the coral framework and its deposition as coral rubble, which results in a high coral content within the mound deposits. The coral mound AR under this scenario is low to moderate (<100 cm kyr^{-1}) and mainly controlled by sediment supply. Such coral rubble-dominated mound deposits are frequently described in the Mediterranean Sea (e.g., Stalder et al., 2015; Titschack et al., 2016; Wang et al., 2019; Corbera et al., 2021) as well as in the Atlantic (Eisele et al., 2008; Frank et al., 2009).

Scenario 2: The coral-derived ecological accommodation space equals sediment supply ($A/S \sim 1$; **Figure 4B**). The fast and sustained growth of corals forming large and densely distributed frameworks results not only in a high baffling capacity but also in a large ecological accommodation space. The sediment supply is constantly high and the coral-derived accommodation space becomes continuously filled. The coral frameworks become quickly buried protecting them from bioerosion and fragmentation and preserving them in life position. This results in a low coral content within the mound deposits but in a high mound AR (>100 cm kyr^{-1}), which is controlled by both the coral-derived ecological accommodation space and the sediment supply. Under such optimal conditions, the hydrodynamic setting has a major influence on the accommodation space and sediment supply, which is directly reflected in the highly variable mound AR. Mound ARs of >300 cm kyr^{-1}, corresponding to an A/S ratio close to 1, reflect the conditions in the record presented here from the coral ridge in the Alborán Sea (see also Fink et al., 2013). Similar high ARs are frequently described from various coral mounds but only during short coral mound formation pulses lasting a few hundred years (e.g., López Correa et al., 2012; Douarin et al., 2013; Stalder et al., 2015; Wienberg et al., 2018). During such formation pulses, ARs are quite close to the annual growth rate of the respective framework-forming coral (∼2–35 millimeters per year; e.g., Larcom et al., 2014; Büscher et al., 2019) and should be therefore close to the upper theoretical limit for mound aggradation (see also Titschack et al., 2015). In contrast, mound ARs of 100–300 cm kyr^{-1} are more frequently encountered in coral mound records (e.g., Frank et al., 2009; Douarin et al., 2013; Wienberg et al., 2018) and reflect less optimal A/S ratios with values slightly above or below 1, suggesting that mound aggradation was limited either by accommodation space or sediment supply, respectively.

Scenario 3: In contrast to the previous two scenarios, in which the environmental conditions for coral proliferation and coral framework development were optimal, scenario 3 is marked by environmental conditions less favorable for corals. The corals survive as scattered colonies but do not form large frameworks. Consequently, their baffling capacity is low to moderate and locally restricted. This results in limited to no coral-derived ecological accommodation space and the predominant bypass of suspended sediments on the coral mound ($0 < A/S << 1$;

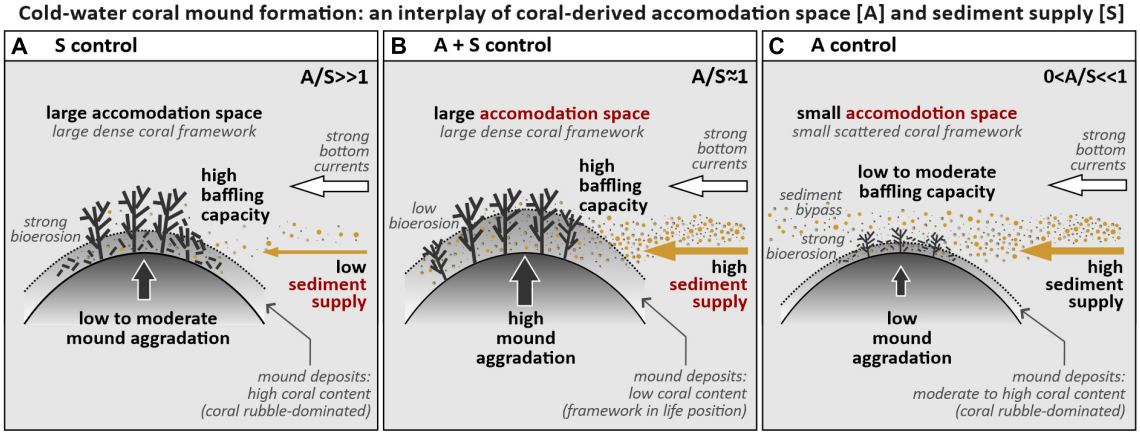

FIGURE 4 | Scheme showing three different scenarios of cold-water coral mound formation and associated mound aggradation rates (ARs) resulting from the interplay between sediment supply (S) and the growth of framework-forming corals providing ecological accommodation space (A). **(A)** The coral-derived A exceeds S (A/S > > 1). Large and densely distributed coral frameworks result in a high baffling capacity and provide large A. As S is too low to completely fill the coral-derived A, the coral frameworks become exposed to bioerosion and fragmentation, which causes their collapse and the deposition of coral rubble (high coral content in mound deposits). The associated AR is low to moderate and mainly controlled by S. **(B)** The coral-derived A is equal to S (A/S∼1). Large and densely distributed coral frameworks result in a high baffling capacity. Due to a high S, the large A provided by the coral frameworks becomes rapidly filled preventing bioerosion and preserving the coral frameworks in life position (low coral content in mound deposits). The associated AR is high and controlled by A and S. **(C)** The coral-derived A is outpaced by S (0 < A/S < < 1). Due to less optimal environmental conditions, only small coral frameworks are present on the mound, which are distributed in a scattered manner and provide only small A. The low to moderate baffling capacity limits the on-mound deposition of current-transported sediments. Consequently, the coral frameworks are largely exposed to bioerosion and fragmentation, which causes their collapse and the deposition of coral rubble (moderate to high coral content in mound deposits). Despite the high S, the associated mound AR is very low as it is mainly controlled by A.

Figure 4C). Consequently, the scattered coral colonies largely remain exposed above the seafloor and are bioeroded and deposited as coral rubble. Despite the high sediment supply, the mound AR is low (<10 cm kyr^{-1}) and mound formation is mainly controlled by the limited coral-derived ecological accommodation space. This scenario is often encountered close to phases of coral mound stagnation, expressed as hiatuses, condensed sections or significant drops in ARs, which are frequently described from various coral mound provinces in the Atlantic and Mediterranean Sea (Dorschel et al., 2005; Rüggeberg et al., 2007; Foubert and Henriet, 2009; Frank et al., 2009; Mienis et al., 2009b; Wienberg et al., 2018; Corbera et al., 2021).

CONCLUSION

Whereas previous comparisons of on- and off-mound surface sediments provided snap-shots of the presence of relatively finer sediments in on-mound settings, the new sediment core-based data presented here, provide a coherent temporal framework and reveal that changing hydrodynamic conditions can shift hemipelagic sediment deposition from off- to on-mound settings and vice versa. However, although the hydrodynamic forcing appears to be the first order control on coral mound formation by providing food and suspended sediment, the complex interplay between the coral framework and sediment deposition has a major impact on the rates of mound aggradation, and hence mound formation.

Coral framework alters the local hydrodynamic regime and its baffling capacity enables fine sediments to settle between the coral branches even under the influence of strong regional hydrodynamics. In addition, it generates ecological accommodation space for sediment deposition. However, while a high baffling capacity merely is the prerequisite for any coral mound formation, the lack of correlation between the enrichment of the on-mound siliciclastic fine sediment fraction and the mound AR clearly points to the interplay of the coral-derived ecological accommodation space (A) controlled by the height/dimension of the coral framework and the sediment supply (S) as additional key factors for mound formation. The record presented here from a coral ridge in the Alborán Sea reveals the efficiency of this interplay. It represents a scenario with an A/S ratio close to 1, allowing for very fast mound aggradation accompanied by an extremely high on-mound accumulation rate of siliciclastic sediments, which is up to ∼25-fold higher compared to the adjacent seafloor at that time. In combination with distinct differences in sediment grain size (coarse sediments off-mound vs. fine sediments on-mound), this points to a bypass situation at the adjacent seafloor triggered by strong hydrodynamics and intense sediment focusing resulting in enhanced deposition of suspended sediments within the coral frameworks of the coral mound.

By comparing our results with other studies from the Mediterranean Sea and the Atlantic Ocean, three scenarios based on the relation of available ecological accommodation space (A) and sediment supply (S) (A/S > > 1; A/S∼1; 0 < A/S < < 1) could be differentiated, which describe their effect on mound formation and coral preservation patterns in coral mound deposits. Furthermore, it is the first application of the sequence

stratigraphic A/S concept (e.g., Homewood et al., 1999) to explain CWC mound formation.

DATA AVAILABILITY STATEMENT

The datasets presented in this study can be found in online repositories. The names of the repository/repositories and accession number(s) can be found below: www.pangaea.de.

AUTHOR CONTRIBUTIONS

DH and JT conceived the study. HW performed the sediment preparation and measurement, including grain size, sediment density, as well as sediment composition. CK prepared the coral sample for the U/Th dating. HW led the writing of the manuscript. All authors supported the interpretation of results and contributed substantially to the final manuscript.

ACKNOWLEDGMENTS

We like to thank the scientific and nautical crews during RV Poseidon cruise POS 385 for on-board assistance. We acknowledge the Deutsche Forschungsgemeinschaft (DFG) for providing ship time for the cruise POS 385 and support through the Cluster of Excellence "The Ocean in the Earth System" and "The Ocean Floor – Earth's Uncharted Interface" (Germany's Excellence Strategy – EXC-2077 – 390741603 of the DFG). The scholarship of HW was funded by the Chinese Scholarship Council. The GeoB Core Repository at the MARUM (Center for Marine Environmental Sciences, University of Bremen, Germany) is acknowledged for providing sediment cores and sample material. Time Fleischmann and Junli Zhang are gratefully acknowledged for their support during the dry bulk density measurements. Brit Kockisch is thanked for her support of the total organic carbon and total carbon measurements. We kindly acknowledge René Eichstädter and Andrea Schröder-Ritzrau for lab support during the Uranium-series dating.

REFERENCES

Bartzke, G., Siemann, L., Büssing, R., Nardone, P., Koll, K., Hebbeln, D., et al. (2021). Investigating the prevailing hydrodynamics around a cold-water coral using a physical and a numerical approach. *Front. Mar. Sci.* 8:663304. doi: 10.3389/fmars.2021.663304

Blum, P. (1997). *Physical Properties Handbook: A Guide to the Shipboard Measurement of Physical Properties of Deep-Sea Cores*. College Station, Texas, USA. Available online at: http://www-odp.tamu.edu

Büscher, J. V., Wisshak, M., Form, A. U., Titschack, J., Nachtigall, K., and Riebesell, U. (2019). In situ growth and bioerosion rates of lophelia pertusa in a norwegian fjord and open shelf cold-water coral habitat. *PeerJ* 7:e7586. doi: 10.7717/peerj.7586

Chang, S., Elkins, C., Alley, M., Eaton, J., and Monismitha, S. (2009). Flow inside a coral colony measured using magnetic resonance velocimetry. *Limnol. Oceanogr.* 54, 1819–1827. doi: 10.4319/lo.2009.54.5.1819

Colman, J. G., Gordon, D. M., Lane, A. P., Forde, M. J., and Fitzpatrick, J. J. (2005). "Carbonate mounds off mauritania, northwest africa: status of deep-water corals and implications for management of fishing and oil exploration activities," in *Cold-Water Corals and Ecosystems*, eds A. Freiwald and J. M. Roberts (Springer), 417–441. doi: 10.1007/3-540-27673-4_21

Corbera, G., Lo Iacono, C., Standish, C. D., Anagnostou, E., Titschack, J., Katsamenis, O., et al. (2021). Glacio-eustatic variations and sapropel events as main controls on the middle pleistocene-holocene evolution of the cabliers coral mound province (W Mediterranean). *Quat. Sci. Rev.* 253:106783. doi: 10.1016/j.quascirev.2020.106783

Cyr, F., Haren, H., Mienis, F., Duineveld, G., and Bourgault, D. (2016). On the influence of cold-water coral mound size on flow hydrodynamics, and vice versa. *Geophys. Res. Lett.* 43, 775–783. doi: 10.1002/2015gl067038

Davies, A. J., Duineveld, G. C., Lavaleye, M. S., Bergman, M. J., van Haren, H., and Roberts, J. M. (2009). Downwelling and deep-water bottom currents as food supply mechanisms to the cold-water coral *Lophelia pertusa* (Scleractinia) at the Mingulay Reef Complex. *Limnol. Oceanogr.* 54, 620–629. doi: 10.4319/lo.2009.54.2.0620

Davies, A. J., and Guinotte, J. M. (2011). Global habitat suitability for framework-forming cold water corals. *PLoS One* 6:e18483. doi: 10.1371/journal.pone.0018483

Davies, A. J., Wisshak, M., Orr, J. C., and Murray Roberts, J. (2008). Predicting suitable habitat for the cold-water coral *Lophelia pertusa* (scleractinia). *Deep Sea Res. Part I Oceanogr. Res. Papers* 55, 1048–1062. doi: 10.1016/j.dsr.2008.04.010

De Clippele, L. H., Huvenne, V. A. I., Orejas, C., Lundälv, T., Fox, A., Hennige, S. J., et al. (2018). The effect of local hydrodynamics on the spatial extent and morphology of cold-water coral habitats at tisler reef, norway. *Coral Reefs* 37, 253–266. doi: 10.1007/s00338-017-1653-y

Dorschel, B., Hebbeln, D., Foubert, A., White, M., and Wheeler, A. J. (2007a). Hydrodynamics and cold-water coral facies distribution related to recent sedimentary processes at Galway Mound west of Ireland. *Mar. Geol.* 244, 184–195. doi: 10.1016/j.margeo.2007.06.010

Dorschel, B., Hebbeln, D., Rüggeberg, A., and Dullo, C. (2007b). Carbonate budget of a cold-water coral carbonate mound: propeller mound, porcupine seabight. *Int. J. Earth Sci.* 96, 73–83. doi: 10.1007/s00531-005-0493-0

Dorschel, B., Hebbeln, D., Ruggeberg, A., Dullo, W., and Freiwald, A. (2005). Growth and erosion of a cold-water coral covered carbonate mound in the Northeast Atlantic during the late Pleistocene and Holocene. *Earth Planetary Sci. Lett.* 233, 33–44. doi: 10.1016/j.epsl.2005.01.035

Douarin, M., Elliot, M., Noble, S. R., Sinclair, D., Henry, L.-A., Long, D., et al. (2013). Growth of north-east Atlantic cold-water coral reefs and mounds during the holocene: a high resolution U-series and 14C chronology. *Earth Planetary Sci. Lett.* 375, 176–187. doi: 10.1016/j.epsl.2013.05.023

Eisele, M., Hebbeln, D., and Wienberg, C. (2008). Growth history of a cold-water coral covered carbonate moundGalway Mound, Porcupine seabight, NE-Atlantic. *Mar. Geol.* 253, 160–169. doi: 10.1016/j.margeo.2008.05.006

Faust, J. C., Stevenson, M. A., Abbott, G. D., Knies, J., Tessin, A., Mannion, I., et al. (2020). Does Arctic warming reduce preservation of organic matter in Barents sea sediments? *Philos. Trans. R. Soc. Mathe. Phys. Eng. Sci.* 378:20190364. doi: 10.1098/rsta.2019.0364

Fentimen, R., Feenstra, E., Rüggeberg, A., Vennemann, T., Hajdas, I., Adatte, T., et al. (2020). Cold-water coral mound archive provides unique insights into intermediate water mass dynamics in the Alboran sea during the last deglaciation. *Front. Mar. Sci.* 7:25.

Fink, H. G., Wienberg, C., De Pol-Holz, R., Wintersteller, P., and Hebbeln, D. (2013). Cold-water coral growth in the Alboran sea related to high productivity during the late pleistocene and holocene. *Mar. Geol.* 339, 71–82. doi: 10.1016/j.margeo.2013.04.009

Flögel, S., Dullo, W. C., Pfannkuche, O., Kiriakoulakis, K., and Rüggeberg, A. (2014). Geochemical and physical constraints for the occurrence of living cold-water corals. *Deep Sea Res. Part II Top. Stud. Oceanogr.* 99, 19–26. doi: 10.1016/j.dsr2.2013.06.006

Flügel, E. (2004). *Microfacies of Carbonate Rocks: Analysis, Interpretation and Application*. Berlin: Springer Science & Business Media.

Foubert, A., Depreiter, D., Beck, T., Maignien, L., Pannemans, B., Frank, N., et al. (2008). Carbonate mounds in a mud volcano province off north-west morocco:

key to processes and controls. *Mar. Geol.* 248, 74–96. doi: 10.1016/j.margeo.2007.10.012

Foubert, A., and Henriet, J.-P. (2009). "Of mounds and cold-water corals," in *Nature and Significance of the Recent Carbonate Mound Record: The Mound Challenger Code*, eds J.-P. Henriet and A. Foubert (Berlin: Springer Berlin Heidelberg), 1–12.

Francois, R., Frank, M., Rutgers van der Loeff, M. M., and Bacon, M. P. (2004). 230Th normalization: an essential tool for interpreting sedimentary fluxes during the late quaternary. *Paleoceanography* 19:PA1018. doi: 10.1029/2003PA000939

Frank, N., Paterne, M., Ayliffe, L., van Weering, T., Henriet, J.-P., and Blamart, D. (2004). Eastern North Atlantic deep-sea corals: tracing upper intermediate water Δ14C during the holocene. *Earth Planetary Sci. Lett.* 219, 297–309. doi: 10.1016/s0012-821x(03)00721-0

Frank, N., Ricard, E., Lutringer-Paquet, A., van der Land, C., Colin, C., Blamart, D., et al. (2009). The holocene occurrence of cold water corals in the NE Atlantic: implications for coral carbonate mound evolution. *Mar. Geol.* 266, 129–142.

Frederiksen, R., Jensen, A., and Westerberg, H. (1992). The distribution of the scleractinian coral *Lophelia pertusa* around the faroe Islands and the relation to internal tidal mixing. *Sarsia* 77, 157–171. doi: 10.1080/00364827.1992.10413502

Freiwald, A. (2002). *Reef-forming Cold-Water Corals, Ocean Margin Systems*. Barlin: Springer, 365–385.

Ginsburg, R. N., and Lowenstam, H. A. (1958). The influence of marine bottom communities on the depositional environment of sediments. *J. Geol.* 66, 310–318. doi: 10.1086/626507

Glogowski, S., Dullo, W.-C., Feldens, P., Liebetrau, V., von Reumont, J., Hühnerbach, V., et al. (2015). The eugen seibold coral mounds offshore western morocco: oceanographic and bathymetric boundary conditions of a newly discovered cold-water coral province. *Geo Mar. Lett.* 35, 257–269.

Guihen, D., White, M., and Lundälv, T. (2013). Boundary layer flow dynamics at a cold-water coral reef. *J. Sea Res.* 78, 36–44.

Hallock, P. (1997). "Reefs and reef limestones in earth history," in *Life and Death of Coral Reefs*, ed. C. Birkeland (Chapman-Hall Science), 13–42.

Heaton, T. J., Köhler, P., Butzin, M., Bard, E., Reimer, R. W., Austin, W. E. N., et al. (2021). marine20the marine radiocarbon age calibration curve (0–55,000 cal BP). *Radiocarbon* 62, 779–820. doi: 10.1017/rdc.2020.68

Hebbeln, D. (2019). "8 Highly variable submarine landscapes in the alborán sea created by cold-water corals," in *Mediterranean Cold-Water Corals: Past, Present and Future: Understanding the Deep-Sea Realms of Coral*, eds C. Orejas and C. Jiménez (Cham: Springer International Publishing), 61–65.

Hebbeln, D., and Samankassou, E. (2015). Where did ancient carbonate mounds growin bathyal depths or in shallow shelf waters? *Earth Sci. Rev.* 145, 56–65. doi: 10.1016/j.earscirev.2015.03.001

Hebbeln, D., Van Rooij, D., and Wienberg, C. (2016). Good neighbours shaped by vigorous currents: cold-water coral mounds and contourites in the North Atlantic. *Mar. Geol.* 378, 171–185. doi: 10.1016/j.margeo.2016.01.014

Hebbeln, D., Wienberg, C., Beuck, L., Freiwald, A., and Wintersteller, P. (2009). Report and preliminary results of RV POSEIDON cruise POS 385 "cold-water corals of the Alboran sea (western mediterranean sea)", faro–toulon, may 29–june 16, 2009. *Berichte Fachbereich Geowissenschaften Univ. Bremen* 273:79.

Hennige, S. J., Larsson, A. I., Orejas, C., Gori, A., De Clippele, L. H., Lee, Y. C., et al. (2021). Using the goldilocks principle to model coral ecosystem engineering. *Proc. R. Soc. B Biol. Sci.* 288:20211260. doi: 10.1098/rspb.2021.1260

Homewood, P., Lafont, F., and Tectonics, C. (1999). *Best Practices in Sequence Stratigraphy for Explorationists and Reservoir Engineers*. Pau: Elf EP, 25.

Huvenne, V. A. I., Masson, D. G., and Wheeler, A. J. (2009). Sediment dynamics of a sandy contourite: the sedimentary context of the darwin cold-water coral mounds, Northern Rockall Trough. *Int. J. Earth Sci.* 98, 865–884. doi: 10.1007/s00531-008-0312-5

Johansen, J. L. (2014). Quantifying water flow within aquatic ecosystems using load cell sensors: a profile of currents experienced by coral reef organisms around Lizard Island, Great Barrier Reef, Australia. *PLoS One* 9:e83240. doi: 10.1371/journal.pone.0083240

Juva, K., Flögel, S., Karstensen, J., Linke, P., and Dullo, W.-C. (2020). Tidal dynamics control on cold-water coral growth: a high-resolution multivariable study on eastern Atlantic cold-water coral sites. *Front. Mar. Sci.* 7:132.

Larcom, E. A., McKean, D. L., Brooks, J. M., and Fisher, C. R. (2014). Growth rates, densities, and distribution of *Lophelia pertusa* on artificial structures in the gulf of Mexico. *Deep Sea Res. Part I Oceanogr. Res. Papers* 85, 101–109. doi: 10.1016/j.dsr.2013.12.005

Lo Iacono, C., Robert, K., Gonzalez-Villanueva, R., Gori, A., Gili, J.-M., and Orejas, C. (2018). Predicting cold-water coral distribution in the cap de creus canyon (NW mediterranean): implications for marine conservation planning. *Prog. Oceanogr.* 169, 169–180. doi: 10.1016/j.pocean.2018.02.012

López Correa, M., Montagna, P., Joseph, N., Rüggeberg, A., Fietzke, J., Flögel, S., et al. (2012). Preboreal onset of cold-water coral growth beyond the arctic circle revealed by coupled radiocarbon and U-series dating and neodymium isotopes. *Quat. Sci. Rev.* 34, 24–43. doi: 10.1016/j.quascirev.2011.12.005

Lowe, R. J., and Falter, J. L. (2015). Oceanic forcing of coral reefs. *Ann. Rev. Mar. Sci.* 7, 43–66. doi: 10.1146/annurev-marine-010814-015834

Mienis, F., Bouma, T. J., Witbaard, R., van Oevelen, D., and Duineveld, G. C. A. (2019). Experimental assessment of the effects of cold-water coral patches on water flow. *Mar. Ecol. Prog. Ser.* 609, 101–117. doi: 10.3354/meps12815

Mienis, F., De Stigter, H. C., De Haas, H., Van der Land, C., and Van Weering, T. C. E. (2012). Hydrodynamic conditions in a cold-water coral mound area on the renard ridge, southern gulf of cadiz. *J. Mar. Syst.* 96-97, 61–71. doi: 10.1016/j.jmarsys.2012.02.002

Mienis, F., de Stigter, H. C., de Haas, H., and van Weering, T. C. E. (2009a). Near-bed particle deposition and resuspension in a cold-water coral mound area at the Southwest rockall trough margin, NE Atlantic. *Deep Sea Res. Part I Oceanogr. Res. Papers* 56, 1026–1038. doi: 10.1016/j.dsr.2009.01.006

Mienis, F., van der Land, C., de Stigter, H. C., van de Vorstenbosch, M., de Haas, H., Richter, T., et al. (2009b). Sediment accumulation on a cold-water carbonate mound at the Southwest rockall trough margin. *Mar. Geol.* 265, 40–50. doi: 10.1016/j.margeo.2009.06.014

Mienis, F., de Stigter, H. C., White, M., Duineveld, G., de Haas, H., and van Weering, T. C. E. (2007). Hydrodynamic controls on cold-water coral growth and carbonate-mound development at the SW and SE rockall trough margin, NE Atlantic Ocean. *Deep Sea Res. Part I Oceanogr. Res. Papers* 54, 1655–1674. doi: 10.1016/j.dsr.2007.05.013

Mienis, F., van Weering, T., de Haas, H., de Stigter, H., Huvenne, V., and Wheeler, A. (2006). Carbonate mound development at the SW rockall trough margin based on high resolution TOBI and seismic recording. *Mar. Geol.* 233, 1–19. doi: 10.1016/j.margeo.2006.08.003

Millot, C., and Taupier-Letag, I. (2005). "Circulation in the mediterranean sea," in *The Mediterranean Sea*, ed. A. Saliot (Berlin: Springer), 29–66. doi: 10.1007/978-94-007-6704-1_3

Mohn, C., Rengstorf, A., White, M., Duineveld, G., Mienis, F., Soetaert, K., et al. (2014). Linking benthic hydrodynamics and cold-water coral occurrences: a high-resolution model study at three cold-water coral provinces in the NE Atlantic. *Prog. Oceanogr.* 122, 92–104. doi: 10.1016/j.pocean.2013.12.003

Monismith, S. G. (2007). Hydrodynamics of coral reefs. *Ann. Rev. Fluid Mecha.* 39, 37–55. doi: 10.1098/rsta.2019.0531

Mullins, H. T., Newton, C. R., Heath, K., and Van Buren, H. M. (1981). Modern deep-water coral mounds north of little bahama bank; criteria for recognition of deep-water coral bioherms in the rock record. *J. Sediment. Res.* 51, 999–1013.

Paull, C. K., Neumann, A. C., Am Ende, B. A., Ussler, W. III, and Rodriguez, N. M. (2000). Lithoherms on the florida–hatteras slope. *Mar. Geol.* 166, 83–101. doi: 10.1126/science.206.4418.515

Pomar, L. (2001). Ecological control of sedimentary accommodation: evolution from a carbonate ramp to rimmed shelf, upper miocene, balearic Islands. *Palaeogeogr. Palaeoclimatol. Palaeoecol.* 175, 249–272. doi: 10.1016/s0031-0182(01)00375-3

Pomar, L., Baceta, J. I., Hallock, P., Mateu-Vicens, G., and Basso, D. (2017). Reef building and carbonate production modes in the west-central tethys during the cenozoic. *Mar. Petrol. Geol.* 83, 261–304. doi: 10.1016/j.marpetgeo.2017.03.015

Pomar, L., and Haq, B. U. (2016). Decoding depositional sequences in carbonate systems: concepts vs experience. *Global Planetary Change* 146, 190–225. doi: 10.1016/j.gloplacha.2016.10.001

Reimer, P. J., and McCormac, F. G. (2002). Marine radiocarbon reservoir corrections for the mediterranean and aegean seas. *Radiocarbon* 44, 159–166. doi: 10.1017/s0033822200064766

Riosmena-Rodriguez, R., Nelson, W., and Aguirre, J. (2016). *Rhodolith/Maerl Beds: A Global Perspective*. Cham: Springer International Publishing.

Roberts, J., Wheeler, A., Freiwald, A., and Cairns, S. (2009). *Cold-water Corals: The Biology and Geology of Deep-Sea Coral Habitats*. Cambridge: Cambridge University Press.

Roberts, J. M., Wheeler, A. J., and Freiwald, A. (2006). Reefs of the deep: the biology and geology of cold-water coral ecosystems. *Science* 312, 543–547.

Rüggeberg, A., Dullo, C., Dorschel, B., and Hebbeln, D. (2007). Environmental changes and growth history of a cold-water carbonate mound (propeller mound, porcupine seabight). *Int. J. Earth Sci.* 96, 57–72. doi: 10.1007/s00531-005-0504-1

Siani, G., Paterne, M., Arnold, M., Bard, E., Métivier, B., Tisnerat, N., et al. (2000). Radiocarbon reservoir ages in the mediterranean sea and black sea. *Radiocarbon* 42, 271–280. doi: 10.1017/s0033822200059075

Siani, G., Paterne, M., Michel, E., Sulpizio, R., Sbrana, A., Arnold, M., et al. (2011). Mediterranean sea surface radiocarbon reservoir age changes since the last glacial maximum. *Science* 294, 1917–1920. doi: 10.1126/science.1063649

Stalder, C., El Kateb, A., Vertino, A., Rüggeberg, A., Camozzi, O., Pirkenseer, C. M., et al. (2018). Large-scale paleoceanographic variations in the western Mediterranean sea during the last 34,000 years: from enhanced cold-water coral growth to declining mounds. *Mar. Micropaleontol.* 143, 46–62. doi: 10.1016/j.marmicro.2018.07.007

Stalder, C., Vertino, A., Rosso, A., Ruggeberg, A., Pirkenseer, C., Spangenberg, J. E., et al. (2015). Microfossils, a key to unravel cold-water carbonate mound evolution through time: evidence from the eastern Alboran sea. *PLoS One* 10:e0140223. doi: 10.1371/journal.pone.0140223

Steinmann, L., Baques, M., Wenau, S., Schwenk, T., Spiess, V., Piola, A. R., et al. (2020). Discovery of a giant cold-water coral mound province along the northern argentine margin and its link to the regional contourite depositional system and oceanographic setting. *Mar. Geol.* 427:106223.

Stuiver, M., Reimer, P. J., and Reimer, R. W. (2021). *CALIB 8.2 [WWW Program]*. Available online at http://calib.org (accessed November 29, 2021).

Tamborrino, L., Wienberg, C., Titschack, J., Wintersteller, P., Mienis, F., Schröder-Ritzrau, A., et al. (2019). Mid-holocene extinction of cold-water corals on the namibian shelf steered by the benguela oxygen minimum zone. *Geology* 47, 1185–1188. doi: 10.1130/G46672.1

Tapia, R., Ho, S. L., Núñez-Ricardo, S., Marchant, M., Lamy, F., and Hebbeln, D. (2021). Increased marine productivity in the southern humboldt current system during MIS 2–4 and 10–11. *Paleoceanogr. Paleoclimatol.* 36:e2020A004066.

Thiem, Ø, Ravagnan, E., Fosså, J. H., and Berntsen, J. (2006). Food supply mechanisms for cold-water corals along a continental shelf edge. *J. Mar. Syst.* 60, 207–219.

Titschack, J., Baum, D., De Pol-Holz, R., López Correa, M., Forster, N., Flögel, S., et al. (2015). Aggradation and carbonate accumulation of holocene norwegian cold-water coral reefs. *Sedimentology* 62, 1873–1898. doi: 10.1111/sed.12206

Titschack, J., Fink, H. G., Baum, D., Wienberg, C., Hebbeln, D., and Freiwald, A. (2016). Mediterranean cold-water corals - an important regional carbonate factory? *Depositional Record* 2, 74–96. doi: 10.1002/dep2.14

Titschack, J., Thierens, M., Dorschel, B., Schulbert, C., Freiwald, A., Kano, A., et al. (2009). Carbonate budget of a cold-water coral mound (challenger mound, IODP exp. 307). *Mar. Geol.* 259, 36–46. doi: 10.1016/j.margeo.2008.12.007

van der Land, C., Eisele, M., Mienis, F., de Haas, H., Hebbeln, D., Reijmer, J. J. G., et al. (2014). Carbonate mound development in contrasting settings on the Irish margin. *Deep Sea Res. Part II Top. Stud. Oceanogr.* 99, 297–306. doi: 10.1016/j.dsr2.2013.10.004

Victorero, L., Blamart, D., Pons-Branchu, E., Mavrogordato, M. N., and Huvenne, V. A. I. (2016). Reconstruction of the formation history of the darwin mounds, N rockall trough: how the dynamics of a sandy contourite affected cold-water coral growth. *Mar. Geol.* 378, 186–195. doi: 10.1016/j.margeo.2015.12.001

Wang, H., Lo Iacono, C., Wienberg, C., Titschack, J., and Hebbeln, D. (2019). Cold-water coral mounds in the southern alboran sea (western mediterranean sea): internal waves as an important driver for mound formation since the last deglaciation. *Mar. Geol.* 412, 1–18. doi: 10.1016/j.margeo.2019.02.007

Wefing, A.-M., Arps, J., Blaser, P., Wienberg, C., Hebbeln, D., and Frank, N. (2017). High precision U-series dating of scleractinian cold-water corals using an automated chromatographic U and Th extraction. *Chem. Geol.* 475, 140–148. doi: 10.1016/j.chemgeo.2017.10.036

Wheeler, A. J., Beyer, A., Freiwald, A., de Haas, H., Huvenne, V. A. I., Kozachenko, M., et al. (2007). Morphology and environment of cold-water coral carbonate mounds on the NW European margin. *Int. J. Earth Sci.* 96, 37–56. doi: 10.1007/s00531-006-0130-6

Wheeler, A. J., Kozachenko, M., Henry, L. A., Foubert, A., de Haas, H., Huvenne, V. A. I., et al. (2011). The moira mounds, small cold-water coral banks in the porcupine seabight, NE Atlantic: part Aan early stage growth phase for future coral carbonate mounds? *Mar. Geol.* 282, 53–64. doi: 10.1016/j.margeo.2010.08.006

Wienberg, C., and Titschack, J. (2017). "Framework-forming scleractinian cold-water corals through space and time: a late quaternary North Atlantic perspective," in *Marine Animal Forests: The Ecology of Benthic Biodiversity Hotspots*, eds S. Rossi, L. Bramanti, A. Gori, and C. Orejas Saco del Valle (Cham: Springer International Publishing), 1–34. doi: 10.1007/978-3-319-17001-5_16-1

Wienberg, C., Titschack, J., Freiwald, A., Frank, N., Lundälv, T., Taviani, M., et al. (2018). The giant mauritanian cold-water coral mound province: oxygen control on coral mound formation. *Quat. Sci. Rev.* 185, 135–152. doi: 10.11646/zootaxa.4878.3.2

Conflict of Interest: The authors declare that the research was conducted in the absence of any commercial or financial relationships that could be construed as a potential conflict of interest.

Publisher's Note: All claims expressed in this article are solely those of the authors and do not necessarily represent those of their affiliated organizations, or those of the publisher, the editors and the reviewers. Any product that may be evaluated in this article, or claim that may be made by its manufacturer, is not guaranteed or endorsed by the publisher.